Original Scientific Paper

Modelling COVID-19 Infection Dynamics in the Presence of Interventions and Environmental Transmission

Farah Naz and Farai Nyabadza*

Abstract

SARS-CoV-2 (COVID-19), a member of the *Betacoronavirus* family, was declared a global pandemic in 2020. This study develops a mathematical model to investigate COVID-19 transmission in a heterogeneous population in South Africa, incorporating environmental transmission and nonpharmaceutical interventions (NPIs) such as mask efficacy. We analyze qualitative properties, including the stability of disease-free and endemic equilibria relative to the basic reproduction number \mathcal{R}_0 . The analysis reveals a transcritical bifurcation at $\mathcal{R}_0 = 1$, indicating that simply reducing \mathcal{R}_0 below one is insufficient for disease elimination. This underscores the need for complementary measures, such as quarantine. Simulations highlight the roles of symptomatic and asymptomatic infections, with reduced mask compliance promoting the persistence of the endemic state. The study concludes that quarantine remains a vital intervention for controlling transmission.

Keywords: SARS-CoV-2, Mathematical model, Non-pharmaceutical interventions, Basic reproduction number, Bifurcation, Simulations.

2020 Mathematics Subject Classification: 92D30; 92B05; 34D20.

How to cite this article

F. Naz, F. Nyabadza, Modelling COVID-19 infection dynamics in the presence of interventions and environmental transmission, Math. Interdisc. Res. 10 (4) (2025) 447-475.

*Corresponding author (E-mail: fnyabadza@uj.ac.za) Academic Editor: Seyfollah Mosazadeh

Received 5 June 2025, Accepted 26 September 2025

DOI: 10.22052/MIR.2025.256993.1524

© 2025 University of Kashan

1. Introduction

On December 31, 2019, the World Health Organization (WHO) reported a cluster of Pneumonia cases in Wuhan, China, caused by the Severe Acute Respiratory Syndrome Coronavirus 2 (SARS-CoV-2), which was later identified as the agent behind Coronavirus disease 2019 (COVID-19). The virus quickly spread globally, prompting the WHO to declare it a pandemic on March 11, 2020 [1]. In the absence of an effective antiviral treatment or vaccine, many countries implemented lockdowns, border closures, and activity restrictions to curb transmission [2]. COVID-19 primarily spreads through respiratory droplets, with symptoms appearing 2–14 days post-exposure, ranging from mild (fever, cough, loss of taste or smell) to severe, requiring hospitalization. Preventive measures include social distancing, handwashing, and wearing face masks [3].

In the absence of vaccines or effective therapeutics, non-pharmacological interventions such as social distancing, contact tracing, and awareness campaigns remain crucial in mitigating the spread of COVID-19. Mathematical modelling has been extensively employed to predict transmission dynamics and evaluate interventions. For instance, compartmental models have been developed to capture provincial and national trends in India (see e.g., [4–6]). Other studies emphasize the influence of vaccination coverage and environmental contamination on outbreak dynamics [7, 8], while media-driven awareness has been shown to significantly reduce transmission [9, 10]. Beyond COVID-19, modelling approaches for related infectious diseases highlight the broader methodological relevance of optimal controls for dengue [11]. Collectively, these studies underscore the indispensable role of mathematical models in elucidating transmission dynamics of COVID-19, guiding intervention strategies, and shaping effective public health policy during pandemics.

Mathematical models have been widely used to study the transmission dynamics and control measures of COVID-19. The SEIR (Susceptible-Exposed-Infected-Recovered) model has been adapted to include factors such as hospitalization, quarantine, and environmental influences [12]. Such models have incorporated seasonality, stochastic infection parameters, and nonlinear dynamics, including chaotic behaviour. A deterministic SEIAQHRM (Susceptible-Exposed-Infected-Asymptomatic-Quarantined-Hospitalised-Recovered) model was developed using a fractal-fractional operator to estimate the reproduction number and transmission rate [13]. However, this model did not consider masked and unmasked individuals. A new SMUEIHR (Susceptible-Masked-Unmasked-Exposed-Infected-Hospitalised-Recovered) model was introduced to analyze the effects of mask usage and hospitalization in reducing transmission rates [14]. However, it did not differentiate between symptomatic and asymptomatic individuals.

In this study, we develop a refined mathematical model to investigate the transmission dynamics of COVID-19 in South Africa, incorporating both symptomatic and asymptomatic infectious groups. The model builds upon and extends existing frameworks by introducing a hybrid structure with improved parameter formu-

lation to more accurately reflect real-world transmission patterns. South Africa, with a population exceeding 59 million, reported its first COVID-19 case on 5 March 2020, and declared a national state of disaster on March 15, 2020 [15]. In response, the government implemented strict Non-Pharmaceutical Interventions (NPIs), including nationwide lockdowns, travel restrictions, and school closures, with measures gradually relaxed in line with infection trends [16]. By November 2020, the country had the highest number of confirmed COVID-19 cases in Africa and ranked fifteenth globally, despite a comparatively low mortality rate [17]. Our model specifically evaluates the effectiveness of key NPIs—particularly mask-wearing and quarantine in mitigating disease spread. The findings can contribute to a broader understanding of public health strategies and their role in reducing transmission and improving health outcomes.

2. Model formulation

We propose a mathematical model to investigate the dynamics of COVID-19 infection, incorporating preventive measures such as mask-wearing and quarantine. The total population at time t, denoted by $\mathcal{N}(t)$, is divided into eight compartments: susceptible S(t), unmasked U(t), masked M(t), exposed E(t), symptomatic infected $I_s(t)$, asymptomatic infected $I_a(t)$, quarantined symptomatic $Q_s(t)$, and recovered R(t). The model, referred to as $(SUMEI_sI_aQ_sR)$, captures the transmission dynamics by classifying individuals based on their infection status and behaviour.

The susceptible class S includes individuals at risk of infection. The masked class M represents those who wear masks, which reduce transmission, while the unmasked class U includes individuals who are not wearing masks, increasing the risk of infection. The exposed class E consists of individuals who are infected but not yet symptomatic. The symptomatic infected class I_s includes individuals with higher viral loads, contributing to increased transmission. The quarantined symptomatic class Q_s accounts for isolated symptomatic individuals, helping with contact tracing and limiting spread. The infected asymptomatic class with I_a represents individuals who are infected but show no symptoms, acting as silent transmitters. The recovered class R includes people who have recovered from infection in all infected categories.

Several key parameters govern the dynamics of the disease: the population recruitment rate (π) , the transition rate between masked and unmasked individuals (α) , and the proportion of individuals who opt to remain unmasked (ρ) . The disease transmission rate is represented by (β) , while (τ) quantifies the efficacy of masks in reducing transmission. The relative infectivity of asymptomatic individuals compared to symptomatic individuals is given by (η) , and the incubation rate (ϵ) dictates the progression from exposed to infected status. The proportion of symptomatic cases is indicated by (κ) , with recovery rates specified for asymptomatic (γ_1) , quarantined symptomatic (γ_2) , and symptomatic individuals (γ_3) .

The general recovery rate for symptomatic individuals is denoted by (ξ) , while the disease-induced death rate is (σ) , and the natural death rate is (μ) .

The force of infection is expressed as:

$$\psi = \beta(I_a + \eta I_s),\tag{1}$$

which reflects the combined contributions of asymptomatic and symptomatic infected individuals to disease transmission. We assume $\eta \geq 1$ to indicate that symptomatic individuals are at least as infectious as asymptomatic ones. The effectiveness of the masks is measured by τ , where $0 \leq \tau \leq 1$. $\tau = 0$, indicates that masks are ineffective, and $\tau = 1$, indicates that the masks are fully effective in preventing disease transmission.

Based on the model diagram, a set of eight non-linear ordinary differential equations representing COVID-19 dynamics in eight compartments of the human population is constructed as follows:

$$\frac{dS}{dt} = \pi - Q_1 S,$$

$$\frac{dU}{dt} = \alpha \rho S - (\mu + \psi)U,$$

$$\frac{dM}{dt} = \alpha (1 - \rho)S - (\mu + (1 - \tau)\psi)M,$$

$$\frac{dE}{dt} = \psi U + (1 - \tau)\psi M - Q_2 E,$$

$$\frac{dI_s}{dt} = \epsilon \kappa E - Q_3 I_s,$$

$$\frac{dI_a}{dt} = \epsilon (1 - \kappa)E - Q_4 I_a,$$

$$\frac{dQ_s}{dt} = \xi I_s - Q_5 Q_s,$$

$$\frac{dR}{dt} = \gamma_1 I_a + \gamma_2 Q_s + \gamma_3 I_s - \mu R,$$
(2)

where

$$\begin{aligned} \mathcal{Q}_1 &= (\mu + \alpha), \quad \mathcal{Q}_2 &= (\mu + \epsilon), \quad \mathcal{Q}_3 &= (\mu + \xi + \gamma_3), \\ \mathcal{Q}_4 &= (\mu + \gamma_1), \qquad \mathcal{Q}_5 &= (\mu + \sigma + \gamma_2). \end{aligned}$$

The model is supplemented by the following initial values:

$$\begin{cases}
S(0) = S_0 > 0, U(0) = U_0 \ge 0, M(0) = M_0 \ge 0, E(0) = E_0 \ge 0, \\
I_s(0) = I_{s_0} \ge 0, I_a(0) = I_{a_0} \ge 0, Q_s(0) = Q_{s_0} \ge 0, R(0) = R_0 \ge 0.
\end{cases}$$
(3)

For all $t \geq 0$, we also set the time t=0 to be the time when COVID-19 started in South Africa. Assume that the initial susceptible population was strictly greater than zero and that no individuals were infected at the onset of the pandemic. The flow chart diagram of the model for the transmission of COVID-19 dynamics in South Africa is designed as Figure 1.

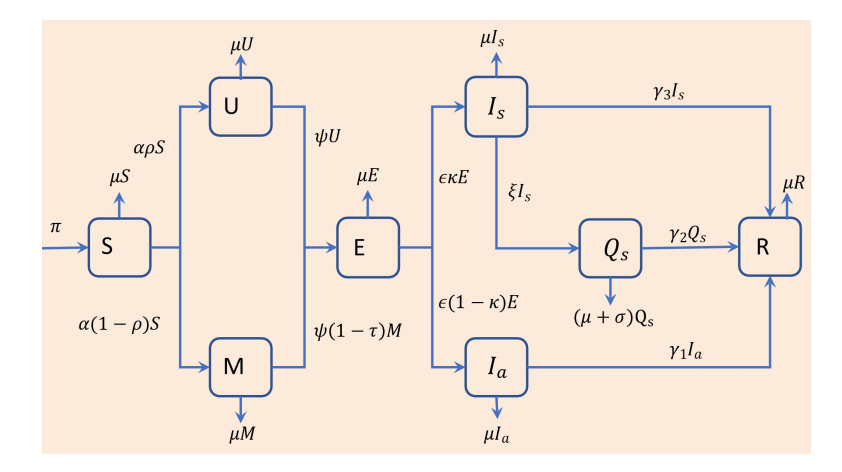


Figure 1: A model diagram for COVID-19 in the presence of mask use and quarantine.

3. Model properties

Well-posedness of the model

In this section, we establish the well-posedness of the model by proving that the basic properties of the model (2), including positivity and boundedness of the solutions, within a biologically feasible region Ω_R for all $t \geq 0$, ensuring the epidemiological relevance of the model.

Positivity of model solutions

The population model is well-posed, as its solutions remain non-negative for all $t \geq 0$, ensuring the biological feasibility of the system. Specifically, for any non-negative initial conditions, all state variables of system (2) remain positive over time, as formally established in the subsequent theorem.

Theorem 3.1. The solutions of the system (2) remain non-negative for the given initial conditions (3) in the region Ω_R for all $t \geq 0$.

Proof. To prove the above theorem, all compartmental variables forming system (2) must be non-negative for all $t \geq 0$. Given that the initial conditions are all

non-negative, considering the susceptible class from system (2)

$$\frac{dS(t)}{dt} = \pi - \mathcal{Q}_1 S(t) \ge -\mathcal{Q}_1 S(t) \ge 0,$$

$$S(t) \ge S_0 \ e^{-\mathcal{Q}_1 t} > 0, \qquad \forall \ t > 0.$$

Since the exponential function is always positive and S(0) > 0, the solution S(t) is guaranteed to remain positive for all t > 0. If $t \to \infty$ then $S(t) \ge 0$. Similarly, from third equation of the system (2), we have

$$\frac{dM}{dt} = \alpha (1 - \rho)S - (\mu + (1 - \tau)\psi)M \ge -(\mu + (1 - \tau)\psi)M \ge 0.$$

Let $t_1 = Sup \{t > 0 : t \in [0, t]\}$, such that t_1 is non-negative, after simplification we get

$$M(t) \ge M_0 e^{\left(-\int_0^{t_1} (1-\tau)\psi dt_1 - \mu t\right)} \ge 0.$$

If t becomes very large, then $M(t) \geq 0$. Similarly, it can be shown that all other variables are non-negative thus, we can say that all system solutions (2) are non-negative for any given non-negative initial conditions for all time $t \geq 0$.

Boundedness of solutions

The model system (2) will be analyzed within the following region:

$$\Omega_R = \left\{ \mathcal{X} \in \Omega_R : 0 \le \mathcal{N}(t) \le \frac{\pi}{\mu} \right\},$$

with

$$\{\mathcal{X} = \{S(t), U(t), M(t), E(t), I_s(t), I_a(t), Q_s(t), R(t)\}\}. \tag{4}$$

The region remains positively invariant within the model system. We have the following theorem to show that these solutions are uniformly unique, bounded, and invariant in the positive feasible region Ω_R .

Theorem 3.2. The solution set (4) of the system (2) with the initial conditions (3) is confined in the positive feasible region Ω_R .

Proof. From the model system (2), we have:

$$\frac{d\mathcal{N}}{dt} \le \pi - \mu \mathcal{N}(t), \quad \forall t \ge 0. \tag{5}$$

Now solving Equation (5) and applying initial conditions, we get:

$$\mathcal{N}(t) \le \frac{\pi}{\mu_0} - \left(\frac{\pi}{\mu} - \mathcal{N}_0\right) e^{-\mu t}.$$
 (6)

If $t \to \infty$ and $\mathcal{N}_0 < \frac{\pi}{\mu}$, then upper bound of $\mathcal{N}(t)$ is $\frac{\pi}{\mu_0}$. If $t \to \infty$ and if $\mathcal{N}_0 \ge \frac{\pi}{\mu}$ then, $\mathcal{N}(t)$ decreases and approaches Ω_R asymptotically. From (6) each state space variable of the system (2) is less than or equal to $\frac{\pi}{\mu_0}$, so the solution set of system (2) is bounded. Thus the system (2) is positively invariant in a closed feasible region Ω_R and all solutions started in this region remain in the Ω_R means,

$$\Omega_R = \left\{ \mathcal{X} \in \Omega_R : 0 \le \mathcal{N}(t) \le \frac{\pi}{\mu} \right\},$$

is positively invariant.

4. Model analysis

In this section, the disease-free equilibrium point, the basic reproductive number, and the endemic equilibrium point are calculated. Stability analysis is established.

Equilibria analysis

The model system (2) has two biologically feasible equilibrium points, namely,

Disease-free equilibrium point $\mathcal{E}_0^* = (S_0^*, U_0^*, M_0^*, E_0^*, I_{s0}^*, I_{a0}^*, Q_{s0}^*, R_0^*)$.

Endemic equilibrium point $\mathcal{E}^{**} = (S^{**}, U^{**}, M^{**}, E^{**}, I_s^{**}, I_a^{**}, Q_s^{**}, R^{**}).$

Disease-free equilibrium point

Disease-free equilibrium is the state where the population is entirely free of disease. The disease-free equilibrium of a system is locally asymptotically stable if $\mathcal{R}_0 < 1$ and unstable when $\mathcal{R}_0 > 1$. Let \mathcal{E}_0^* be the disease-free equilibrium point, then for the system (2). We obtained the disease-free equilibrium by setting the right-hand side equal to zero. We get eight homogeneous equations.

$$\pi - Q_{1}S^{*} = 0,$$

$$\alpha \rho_{u}^{*}S^{*} - (\mu + \psi^{*})U^{*} = 0,$$

$$\alpha (1 - \rho_{u}^{*})S^{*} - (\mu + (1 - \tau)\psi^{*})M^{*} = 0,$$

$$\psi^{*}U^{*} + (1 - \tau)\psi^{*}M^{*} - Q_{2}E^{*} = 0,$$

$$\epsilon \kappa E^{*} - Q_{3}I_{s}^{*} = 0,$$

$$\epsilon (1 - \kappa)E^{*} - Q_{4}I_{a}^{*} = 0,$$

$$\xi I_{s}^{*} - Q_{5}Q_{s}^{*} = 0,$$

$$\gamma_{1}I_{a}^{*} + \gamma_{2}Q_{s}^{*} + \gamma_{3}I_{s}^{*} - \mu R^{*} = 0.$$
(7)

From the above system (7), we get the following:

$$S^* = \frac{\pi}{Q_1}, \quad U^* = \frac{\alpha \pi \rho}{Q_1(\mu + I_s^* \phi_5)}, \quad M^* = \frac{\alpha \pi (1 - \rho)}{Q_1(\mu + (1 - \tau)I_s^* \phi_5)},$$

$$E^* = \phi_2 I_s^*, \quad I_a^* = \phi_3 I_s^*, \quad Q_s^* = \phi_1 I_s^*, \quad R^* = \phi_4 I_s^*, \quad \psi^* = \phi_5 I_s^*.$$
(8)

with

$$\phi_1 = \frac{\xi}{\mathcal{Q}_5}, \quad \phi_2 = \frac{\mathcal{Q}_3}{\epsilon \kappa}, \quad \phi_3 = \frac{\epsilon(1-\kappa)\phi_2}{\mathcal{Q}_4}, \quad \phi_4 = \frac{\gamma_3 + \gamma_2\phi_1 + \gamma_1\phi_3}{\mu}, \quad \phi_5 = \beta(\phi_3 + \eta). \tag{9}$$

Using (8) and (9) in the system (7) we get the following:

$$I_s^* \left(-Q_2 \phi_2 + \frac{\pi \alpha \phi_5 \left(\mu + \mu(-1 + \rho)\tau + (1 - \tau)I_s \phi_5 \right)}{Q_1 \left(\mu + I_s \phi_5 \right) \left(\mu + (1 - \tau)I_s \phi_5 \right)} \right) = 0.$$
 (10)

At disease-free equilibrium $I_s^* = 0$, then from (8), we get $E^* = I_a^* = Q_s^* = R^* = 0$, which gives

$$S_0^* = \frac{\pi}{Q_1}, \quad U_0^* = \frac{\alpha \rho \pi}{\mu Q_1}, \quad M_0^* = \frac{\alpha (1 - \rho) \pi}{\mu Q_1}.$$

Thus, the disease-free equilibrium point is summarized below \mathcal{E}_0^* , is given by

$$\left(S_0^*, \ U_0^*, \ M_0^*, \ E_0^*, \ I_{s0}^*, \ I_{a0}^*, \ Q_{s0}^*, \ R_0^*\right) = \left(\frac{\pi}{Q_1}, \ \frac{\alpha\pi\rho}{\mu Q_1}, \ \frac{\alpha(1-\rho)\pi}{\mu Q_1}, \ 0, \ 0, \ 0, \ 0, \ 0\right).$$
(11)

Basic reproduction number

In epidemiological models, the basic reproduction number, denoted as (\mathcal{R}_0) , represents the average number of secondary infections caused by a single infectious individual introduced into a fully susceptible population [18]. Using the next-generation method for the model system (2), the basic reproduction number, $\mathcal{R}_0 = \mathcal{R}(\tau)$, is determined as the dominant eigenvalue of the next-generation matrix, $\mathcal{K} = FV^{-1}$. Here, F represents the rate of new infections, while V denotes the rate of transfer of individuals into or out of exposed and infectious compartments [19]. We write new infection terms as F = F(x) and all other transfer terms as V = V(x). At the disease-free equilibrium (DFE), we have

$$U_0^* = \frac{\alpha \rho^* \pi}{\mu Q_1}, \quad M_0^* = \frac{\alpha (1 - \rho^*) \pi}{\mu Q_1}.$$

So for construction of F and V we have the following:

$$\frac{dE}{dt} = \psi U + (1 - \tau)\psi M - \mathcal{Q}_2 E,$$

$$\frac{dI_s}{dt} = \epsilon \kappa E - \mathcal{Q}_3 I_s,$$

$$\frac{dI_a}{dt} = \epsilon (1 - \kappa)E - Q_4 I_a,$$

$$\frac{dQ_s}{dt} = \xi I_s - Q_5 Q_s.$$

Let us define $\mathcal{L} = U_0^* + (1 - \tau)$, $M_0^* = \frac{\alpha \pi \mathcal{Q}_{00}}{\mu \mathcal{Q}_1}$, where; $\mathcal{Q}_{00} = (1 - \tau(1 - \rho))$. Now jacobians at DFE with state order E, I_s, I_a, Q_s are given:

The reproductive number for COVID-19 with non-pharmaceutical interventions such as masks is given as the spectral radius of the matrix $\mathcal{K} = FV^{-1}$. The largest eigenvalue of \mathcal{K} , after some algebraic manipulation, can be written as a sum of two sub-reproduction numbers so that

$$\mathcal{R}_0 = \frac{\beta \, \epsilon \mathcal{L}}{\mathcal{Q}_2} \left(\frac{(1-\kappa)}{\mathcal{Q}_4} + \frac{\eta \, \kappa}{\mathcal{Q}_3} \right) = \frac{\beta \, \epsilon}{\mathcal{Q}_2} \, \frac{\alpha \pi \mathcal{Q}_{00}}{\mathcal{Q}_1 \mu} \, \left(\frac{(1-\kappa)}{\mathcal{Q}_4} + \frac{\eta \, \kappa}{\mathcal{Q}_3} \right).$$

 $Q_{00}=(1-\tau(1-\rho))=\rho+(1-\tau)(1-\rho)$, represents the effective fraction of susceptibles contributing to transmission. If $\tau=1$, then masks provide perfect protection, and if $\rho=1$, means everyone is unmasked. Which shows explicitly how mask coverage $(1-\rho)$ and mask efficacy (τ) reduce the basic reproduction number.

Hence,

$$\mathcal{R}_0 = \mathcal{R}_a + \mathcal{R}_s$$

with,

$$\mathcal{R}_{a} = \frac{\alpha\beta\pi\epsilon(1-\kappa)\Big(\rho + (1-\tau)(1-\rho)\Big)}{\mu\mathcal{Q}_{1}\mathcal{Q}_{2}\mathcal{Q}_{4}}, \quad \mathcal{R}_{s} = \frac{\alpha\beta\pi\epsilon\eta\kappa(\Big(\rho + (1-\tau)(1-\rho)\Big)}{\mu\mathcal{Q}_{1}\mathcal{Q}_{2}\mathcal{Q}_{3}}.$$
(12)

The expression \mathcal{R}_a represents the contributions of the asymptomatic individuals, and the expression \mathcal{R}_s represents the contributions of the symptomatic individuals.

Endemic equilibrium

After some algebraic manipulation, the endemic equilibrium (EE) \mathcal{E}^{**} is given by

$$\mathcal{E}^{**} = (S^{**}, U^{**}, M^{**}, E^{**}, I_s^{**}, I_a^{**}, Q_s^{**}, R^{**}).$$

Let

$$\psi^{**} = \beta (I_a^{**} + \eta I_s^{**}),$$

denote the endemic force of infection. Let

$$\mathcal{L} = \frac{\eta \kappa}{\mathcal{Q}_3} + \frac{1-\kappa}{\mathcal{Q}_4}, \qquad \mathcal{Q}_{00} = \rho + (1-\tau)(1-\rho).$$

From the steady-state relations and the definition of \mathcal{R}_0

$$\mathcal{R}_0 = \frac{\alpha \beta \pi \epsilon \, \mathcal{Q}_{00} \, \mathcal{L}}{\mu \, \mathcal{Q}_1 \, \mathcal{Q}_2} \,.$$

Let

$$\Delta = \rho + (1 - \tau)^2 (1 - \rho), \qquad \psi^{**} = \frac{\mu \mathcal{Q}_{00}}{\Delta \mathcal{R}_0} (\mathcal{R}_0 - 1), \qquad (\mathcal{R}_0 \ge 1).$$

We obtain the endemic state valid for $\mathcal{R}_0 \geq 1$ as follows:

$$S^{**} = \frac{\pi}{\mathcal{Q}_1}, \qquad U^{**} = \frac{\alpha\pi\rho\mathcal{R}_0\Delta}{\mu\mathcal{Q}_1\Big(\mathcal{R}_0\Delta + \mathcal{Q}_{00}\left(\mathcal{R}_0 - 1\right)\Big)},$$

$$M^{**} = \frac{\alpha\pi(1-\rho)\mathcal{R}_0\Delta}{\mu\mathcal{Q}_1\Big(\mathcal{R}_0\Delta + (1-\tau)\mathcal{Q}_{00}\left(\mathcal{R}_0 - 1\right)\Big)}, \qquad E^{**} = \frac{\mu\mathcal{Q}_{00}\left(\mathcal{R}_0 - 1\right)}{\beta\epsilon\mathcal{L}\Delta\mathcal{R}_0},$$

$$I_s^{**} = \frac{\mu\kappa\mathcal{Q}_{00}\left(\mathcal{R}_0 - 1\right)}{\beta\mathcal{Q}_3\mathcal{L}\Delta\mathcal{R}_0}, \qquad I_a^{**} = \frac{\mu\left(1-\kappa\right)\mathcal{Q}_{00}\left(\mathcal{R}_0 - 1\right)}{\beta\mathcal{Q}_4\mathcal{L}\Delta\mathcal{R}_0},$$

$$Q_s^{**} = \frac{\xi\kappa\mu\mathcal{Q}_{00}\left(\mathcal{R}_0 - 1\right)}{\beta\mathcal{Q}_3\mathcal{Q}_5\mathcal{L}\Delta\mathcal{R}_0}, \qquad R^{**} = \frac{\mathcal{Q}_{00}\mathcal{H}\left(\mathcal{R}_0 - 1\right)}{\beta\mathcal{L}\Delta\mathcal{R}_0},$$
 with
$$\mathcal{H} = \frac{\gamma_1(1-\kappa)\mathcal{Q}_3\mathcal{Q}_5 + \gamma_3\kappa\mathcal{Q}_4\mathcal{Q}_5 + \gamma_2\xi\kappa\mathcal{Q}_4}{\mathcal{Q}_3\mathcal{Q}_4\mathcal{Q}_5}.$$

Stability analysis

In this section, we analyze the stability properties of the model. The local stability of the disease-free equilibrium (DFE) is investigated using the Routh–Hurwitz criteria, while the local stability of the endemic equilibrium is examined with the center manifold theory. For the global stability of the endemic equilibrium, an appropriately constructed Lyapunov function is employed. Furthermore, bifurcation analysis is carried out to determine the conditions under which qualitative changes in the system occur. In particular, a transcritical bifurcation is observed at $\mathcal{R}_0 = 1$, indicating an exchange of stability between the DFE and the endemic equilibrium. This bifurcation highlights that a reproduction number less than

unity alone may be insufficient to eliminate the disease, emphasizing the need for complementary control measures, such as quarantine and mask compliance, to ensure effective disease management. The equilibrium point of a dynamical system is said to be stable if all solutions converge to the equilibrium point within an invariant region; see, for instance, [20].

Local stability of disease-free equilibrium point \mathcal{E}_0^*

Theorem 4.1. The model system (2) is locally asymptotically stable (LAS) at the disease-free equilibrium point \mathcal{E}_0^* if $\mathcal{R}_0 < 1$ and unstable otherwise.

Proof. To check local stability for disease-free equilibrium point $\mathcal{E}_{\mathbf{0}}^*$ the system (2) is linearized to obtain the Jacobian matrix $\mathcal{J}(\mathcal{E}_{\mathbf{0}}^*)$ as follows:

$$\psi = \beta(I_a + \eta I_s).$$

The Jacobian matrix $\mathcal{J}(\mathcal{E}_0^*)$ becomes

$$\mathcal{J}(\mathcal{E}_{\mathbf{0}}^{*}) = \begin{pmatrix}
-Q_{1} & 0 & 0 & 0 & 0 & 0 & 0 & 0 & 0 \\
\alpha\rho_{u} & -\mu & 0 & 0 & -\beta\eta U_{0} & -\beta U_{0} & 0 & 0 \\
\alpha(1-\rho_{u}) & 0 & -\mu & 0 & -\beta\eta(1-\tau)M_{0} & -\beta(1-\tau)M_{0} & 0 & 0 \\
0 & 0 & 0 & -Q_{2} & \beta\eta(U_{0}+(1-\tau)M_{0}) & \beta(U_{0}+(1-\tau)M_{0}) & 0 & 0 \\
0 & 0 & 0 & \epsilon\kappa_{s} & -Q_{3} & 0 & 0 & 0 \\
0 & 0 & 0 & \epsilon(1-\kappa_{s}) & 0 & -Q_{4} & 0 & 0 \\
0 & 0 & 0 & 0 & \xi & 0 & -Q_{5} & 0 \\
0 & 0 & 0 & 0 & \gamma_{3} & \gamma_{1} & \gamma_{2} & -\mu \\
\end{cases} .$$

All the eigenvalues of the Jacobian matrix $\mathcal{J}(\mathcal{E}_{\mathbf{0}}^*)$, must be negative to prove the local stability of the system at the DFE point. The eigenvalues of $\mathcal{J}(\mathcal{E}_{\mathbf{0}}^*)$ are $\lambda_1 = -\mathcal{Q}_1$, $\lambda_2 = -\mathcal{Q}_5$, $\lambda_3 = \lambda_4 = \lambda_5 = -\mu$ and

$$a\lambda^3 + b\lambda^2 + c\lambda + d = 0, (14)$$

with

$$a = 1,$$

$$b = \mathcal{Q}_2 + \mathcal{Q}_3 + \mathcal{Q}_4,$$

$$c = \mathcal{Q}_2 \mathcal{Q}_3 + \mathcal{Q}_2 \mathcal{Q}_4 + \mathcal{Q}_3 \mathcal{Q}_4 - \left(\frac{\mathcal{Q}_6 \mathcal{Q}_7}{\mathcal{Q}_1}\right),$$

$$d = \mathcal{Q}_2 \mathcal{Q}_3 \mathcal{Q}_4 (1 - \mathcal{R}_0),$$

$$(15)$$

where, $Q_6 = \left((1-\kappa) + \eta\kappa\right)$ and $Q_7 = \left(\frac{\alpha\beta\pi\epsilon}{\mu}\right)$ and to be certain about the nature of the roots in Equation (14), the second half of this equation leads us to a polynomial of degree three. The Routh-Hurwitz criteria have been used to solve this cubic polynomial.

Definition 4.2. The Routh-Horwitz criteria are used to examine the nature of the roots of the polynomials. By [21], the Routh-Hurwitz criteria, the solution set

$$X = \{S(t), U(t), M(t), E(t), I_s(t), I_a(t), Q_s(t), R(t)\},$$

of the system is stable if all real roots λ of the characteristic equation lie in the left-hand complex plane, meaning $Re\lambda < 0$ for all roots λ .

Clearly, b > 0, and obviously, d > 0 if $\mathcal{R}_0 < 1$. Now, solving for (bc - d), we obtain the following result:

$$bc - d = (\mathcal{Q}_2 + \mathcal{Q}_3 + \mathcal{Q}_4) \left[\mathcal{Q}_2 \mathcal{Q}_4 (1 - \mathcal{R}_a) + \mathcal{Q}_2 \mathcal{Q}_3 (1 - \mathcal{R}_s) \right]$$

$$+ \mathcal{Q}_3 \mathcal{Q}_4 (\mathcal{Q}_3 + \mathcal{Q}_4) + \mathcal{Q}_2 \mathcal{Q}_3 \mathcal{Q}_4 \mathcal{R}_0 > 0.$$

$$(16)$$

We conclude that b.c-d>0, if and only if $\mathcal{R}_a<1$, $\mathcal{R}_s<1$ and $\mathcal{R}_0<1$. All the conditions of Routh-Horwitz's criteria are satisfied, indicating that all the complex roots λ are negative and lie in the left-half plane. Thus, the characteristic Equation (14) has only negative roots, which ensures that the system is locally asymptotically stable (LAS) at the disease-free equilibrium point (DFE).

Local stability of endemic equilibrium point \mathcal{E}^{**}

Theorem 4.3. The model system (2) is locally asymptotically stable (LAS) around the endemic equilibrium point \mathcal{E}^{**} for $\mathcal{R}_0 > 1$. Also system (2) experiences a backward bifurcation at $\mathcal{R}_0 > 1$.

Proof. To investigate the local asymptotic stability of the endemic equilibrium point \mathcal{E}^{**} , we use the theory of center manifold.

Let us re-write our system (2) by using the notations $S(t)=x_1,\,U(t)=x_2$, $M(t)=x_3$, $E(t)=x_4$, $I_s(t)=x_5$, $I_a(t)=x_6$, $Q_s(t)=x_7$, $R(t)=x_8$. By using vector notation $x=(x_1,x_2,x_3,x_4,x_5,x_6,x_7,x_8)^T$. The model system (2) can be written in the form $\frac{dx}{dt}=f(x)$ with

$$f = (f_1, f_2, f_3, f_4, f_5, f_6, f_7, f_8)^T,$$

as follows:

$$\dot{x}_{1} = f_{1} = \pi - (\mu + \alpha)x_{1},
\dot{x}_{2} = f_{2} = \alpha\rho x_{1} - \beta(x_{6} + \eta x_{5})x_{2} - \mu x_{2},
\dot{x}_{3} = f_{3} = \alpha(1 - \rho)x_{1} - \beta(1 - \tau)(x_{6} + \eta x_{5})x_{3} - \mu x_{3},
\dot{x}_{4} = f_{4} = \beta(x_{6} + \eta x_{5})x_{2} + \beta(1 - \tau)(x_{6} + \eta x_{5})x_{3} - \mathcal{Q}_{2}x_{4},
\dot{x}_{5} = f_{5} = \epsilon \kappa x_{4} - \mathcal{Q}_{3}x_{5},
\dot{x}_{6} = f_{6} = \epsilon(1 - \kappa)x_{4} - (\mu + \gamma_{1})x_{6},
\dot{x}_{7} = f_{7} = \xi x_{5} - \mathcal{Q}_{5}x_{7},
\dot{x}_{8} = f_{8} = \gamma_{1}x_{6} + \gamma_{2}x_{7} + \gamma_{3}x_{5} - \mu x_{8}.$$

$$(17)$$

We consider the disease transmission rate β_b^* as a bifurcation parameter, $\beta = \beta_b^*$ corresponding to $\mathcal{R}_0 = 1$, is

$$\beta_b^* = \frac{\mu \mathcal{Q}_1 \mathcal{Q}_2 \mathcal{Q}_3 \mathcal{Q}_4}{\alpha \pi \epsilon (\rho \tau + (1 - \tau))(\mathcal{Q}_3 (1 - \kappa) + \eta \mathcal{Q}_4 \kappa)}.$$
 (18)

The system Equation (17) has a simple eigenvalue with zero real part, and all the other eigenvalues are negative (which means it has a hyperbolic equilibrium point). Thus, centre manifold theory can be used to analyze the dynamics of the system (17) near $\beta = \beta_b^*$, by using the approach as in [22]. The Jacobian matrix of the transformed system (17) evaluated at disease free equilibrium (\mathcal{E}_0) for COVID-19, denoted by $J^*(\mathcal{E}_0)$ and given by

$$J^*(\mathcal{E}_0) = \begin{pmatrix} -\alpha - \mu & 0 & 0 & 0 & 0 & 0 & 0 & 0 & 0 \\ \alpha \rho_u & -\mu - \beta x_9 & 0 & 0 & -\beta \eta x_2 & -\beta x_2 & 0 & 0 \\ \alpha (1 - \rho_u) & 0 & -\mu - \beta (1 - \tau) x_9 & 0 & -\beta \eta (1 - \tau) x_3 & -\beta (1 - \tau) x_3 & 0 & 0 \\ 0 & \beta x_9 & \beta (1 - \tau) x_9 & -\mathcal{Q}_2 & \beta \eta x_2 + \beta \eta (1 - \tau) x_3 & \beta (x_2 + (1 - \tau) x_3) & 0 & 0 \\ 0 & 0 & 0 & \epsilon \kappa_s & -\mathcal{Q}_3 & 0 & 0 & 0 \\ 0 & 0 & 0 & \epsilon (1 - \kappa_s) & 0 & -\mathcal{Q}_4 & 0 & 0 \\ 0 & 0 & 0 & 0 & \xi & 0 & -\mathcal{Q}_5 & 0 \\ 0 & 0 & 0 & 0 & \xi & 0 & -\mathcal{Q}_5 & 0 \\ 0 & 0 & 0 & 0 & 0 & \gamma_3 & \gamma_1 & \gamma_2 & -\mu \end{pmatrix},$$

$$(19)$$

where,

$$x_9 = (\eta x_5 + x_6), \quad \mathcal{Q}_2 = (\mu + \epsilon), \quad \mathcal{Q}_3 = (\mu + \xi + \gamma_3), \quad \mathcal{Q}_4 = (\mu + \gamma_1), \quad \mathcal{Q}_5 = (\mu + \sigma + \gamma_2).$$

At disease-free equilibrium, we have

$$x_1 = \frac{\pi}{\mathcal{Q}_1}, \quad x_2 = \frac{\alpha \pi \rho}{\mu \mathcal{Q}_1}, \quad x_3 = \frac{\alpha \pi (1 - \rho)}{\mu \mathcal{Q}_1}, \quad x_4 = x_5 = x_6 = x_7 = x_8 = 0.$$

The right eigenvector $w = (w_1, w_2, w_3, w_4, w_5, w_6, w_7, w_8)^{\top}$, associated with zero eigenvalues of the jacobian matrix such that $J^*(\mathcal{E}_0).w = 0$, at $\beta = \beta_b^*$ with $w_4 = 1$ is

$$(w_1, w_2, w_3, w_4, w_5, w_6, w_7, w_8)^{\top} = \left(0, \frac{-\mathcal{Q}_2 \rho}{\mu(1 - \tau + \rho \tau)}\right), \frac{\mathcal{Q}_2(1 - \tau)(1 - \rho)}{\mu(1 - \tau + \rho \tau)}, 1, \frac{\epsilon \kappa}{\mathcal{Q}_3}, \frac{\epsilon(1 - \kappa)}{\mathcal{Q}_4}, \frac{\epsilon \xi \kappa}{\mathcal{Q}_5 \mathcal{Q}_3}, \left(\frac{\epsilon \gamma_1(1 - \kappa)}{\mu \mathcal{Q}_4} + \frac{\epsilon(\xi \gamma_2 + \gamma_3 \mathcal{Q}_5)}{\mu \mathcal{Q}_5 \mathcal{Q}_3}\right)\right).$$

Similarly, we find the left eigen-vector $v = (v_1, v_2, v_3, v_4, v_5, v_6, v_7, v_8)$, such that $J^*(\mathcal{E}_0)$ associated with zero eigenvalue and with

$$v_4 = \frac{\mathcal{Q}_4 \mathcal{Q}_3 [\mathcal{Q}_3 (1 - \kappa) + \eta \mathcal{Q}_4 \kappa]}{\mathcal{Q}_2 [\mathcal{Q}_3^2 (1 - \kappa) + \eta \mathcal{Q}_4^2 \kappa]}.$$

The left eigenvector $(v_1, v_2, v_3, v_4, v_5, v_6, v_7, v_8)$ is as follows

$$\left(0,0,0,\frac{\mathcal{Q}_4\mathcal{Q}_3[\mathcal{Q}_3(1-\kappa)+\eta\mathcal{Q}_4\kappa]}{\mathcal{Q}_2[\mathcal{Q}_3^2(1-\kappa)+\eta\mathcal{Q}_4^2\kappa]},\frac{\eta\mathcal{Q}_4^2\mathcal{Q}_3}{\epsilon[\mathcal{Q}_3^2(1-\kappa)+\eta\mathcal{Q}_4^2\kappa]},\frac{\mathcal{Q}_4\mathcal{Q}_3^2}{\epsilon[\mathcal{Q}_3^2(1-\kappa)+\eta\mathcal{Q}_4^2\kappa]},0,0\right).$$

The right-eigenvector w and left-eigenvector v satisfy the condition v.w = 1. Now we compute the following non-zero second-order partial derivatives of the system (17) at the disease-free equilibrium point.

Now we compute the coefficients a and b as in [22]. By substituting the values of all non-zero second-order partial derivatives and the left and right eigen vectors from the above system at the threshold value $\beta = \beta_b^*$, we obtain

$$a = \sum_{k,i,j=1}^{8} v_k w_i w_j \frac{\partial^2 f_k(\beta_1^*, \varepsilon_0^*)}{\partial x_i \partial x_j} = 2\beta v_4 (\eta w_5 + w_6) (w_3 (1 - \tau) + w_2).$$
 (20)

The second bifurcation coefficient b is given by

$$b = \sum_{k,j=1}^{8} v_k w_j \frac{\partial^2 f_k(\varepsilon_0^*, \beta_1^*)}{\partial x_i \partial \beta_m} = v_4 [(x_6 + \eta x_5)(w_3(1 - \tau) + w_2) + (w_6 + \eta w_5)(x_2 + (1 - \tau)x_3)]. \tag{21}$$

From the above expressions, we observe that b is always positive; according to remark 1 in Theorem 4.1 from [22], the system (17) exhibits bifurcation phenomena if the bifurcation coefficient a is positive. The positivity of a, holds if

$$\kappa < \frac{\mathcal{Q}_3}{\mathcal{Q}_3 - \eta \mathcal{Q}_4},\tag{22}$$

provides a necessary condition for the occurrence of bifurcation. This concludes that the system exhibits a transcritical bifurcation at the basic reproduction number $\mathcal{R}_0 = 1$. Hence, as in [4] we conclude that the endemic equilibrium point \mathcal{E}^{**} is locally asymptotically stable for $\mathcal{R}_0 > 1$.

The bifurcation analysis

Bifurcation analysis is performed to investigate qualitative changes in system dynamics. In particular, a transcritical bifurcation occurs at $\mathcal{R}_0 = 1$, indicating an exchange of stability between the DFE and the endemic equilibrium. This result implies that reducing \mathcal{R}_0 below unity is necessary but may not be sufficient for the elimination of disease, highlighting the importance of complementary control measures, such as effective quarantine and high compliance with masks, to ensure a controlled epidemic. Figure 2 provides a graphical representation of forward bifurcation, while Figure 3 illustrates the backward bifurcation. These visualizations are based on the parameter values specified in the respective captions. The

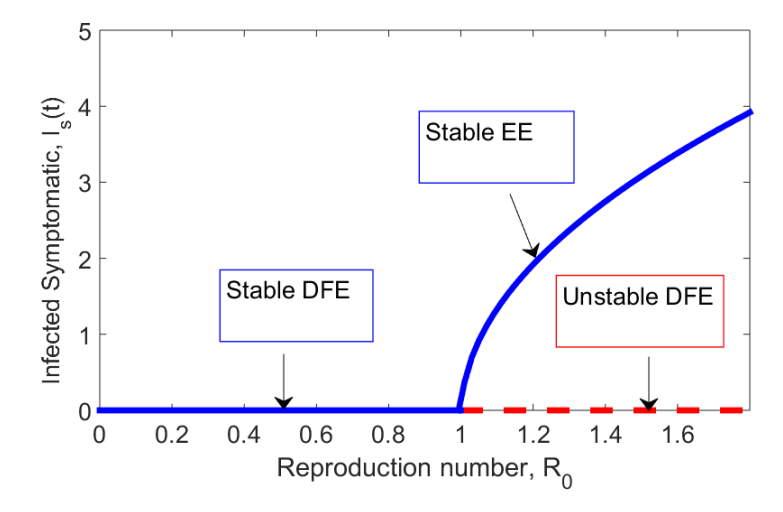


Figure 2: Forward bifurcation: $\pi=28.6,\ \mu=0.436,\ \alpha=0.69,\ \rho=0.582,$ $\beta=0.082,\ \eta=1.496,\ \tau=0.458,\ \epsilon=0.41,\ \kappa=0.336,\ \xi=0.12,\ \gamma_3=0.064,$ $\sigma=0.434,\ \gamma_2=0.184,\ \gamma_1=0.27.$

model system (2) exhibits a transcritical bifurcation at $\mathcal{R}_0 = 1$, with a forward bifurcation for $\mathcal{R}_0 > 1$ indicating disease persistence. However, the Figure 3 explains the presence of a backward bifurcation where both disease-free and endemic equilibria coexist for $\mathcal{R}_0^c < \mathcal{R}_0 < 1$, which means that reducing \mathcal{R}_0 below 1 alone is insufficient for eradication. In such scenarios, mask usage must be complemented by additional interventions such as social distancing, public awareness, isolation of cases, and effective case detection. The influence of mask efficacy, denoted by τ , on disease dynamics is demonstrated in Figure 4. We observe that an increase in τ facilitates better control over the spread of COVID-19. This aligns with our model's objective, demonstrating that masks play a crucial role in mitigating the rapid transmission of the disease.

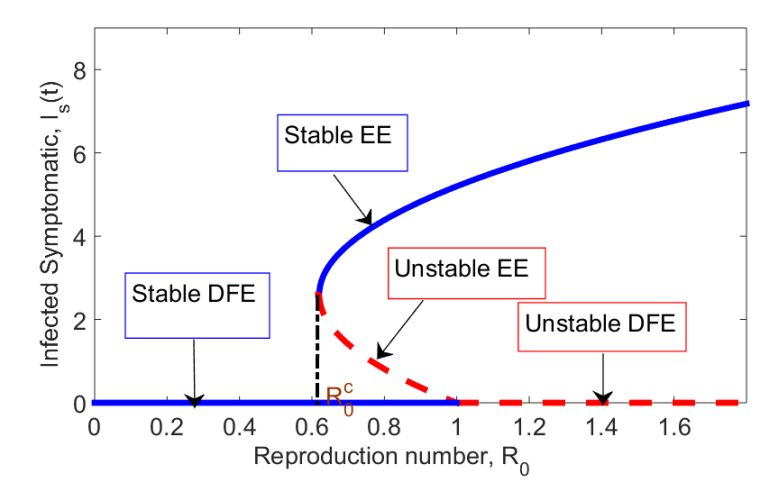


Figure 3: Backward bifurcation: $\pi=32.4,~\mu=0.358,~\alpha=0.675,~\rho=0.582,~\beta=0.071,~\eta=1.44,~\tau=0.6,~\epsilon=0.715,~\kappa=0.336,~\xi=0.12,~\gamma_3=0.064,~\sigma=0.434,~\gamma_2=0.184,~\gamma_1=0.27.$

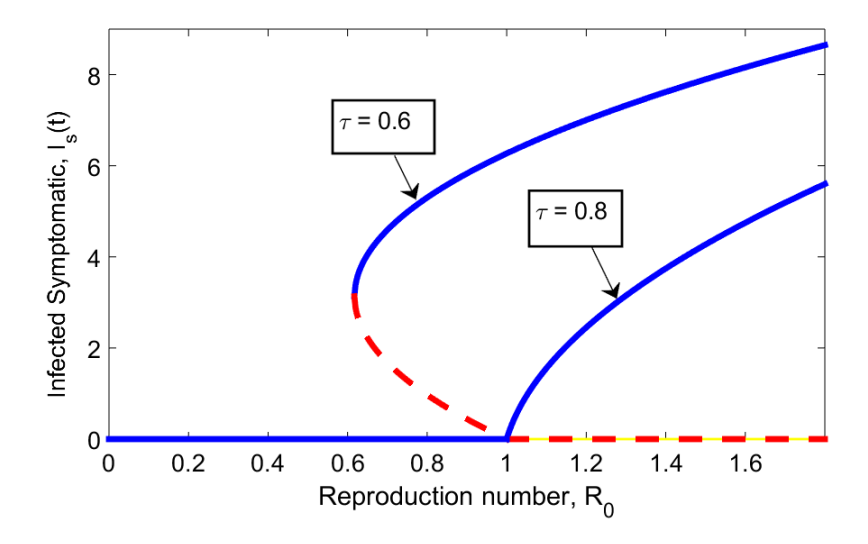


Figure 4: Effect of τ on the bifurcation behaviour of model dynamics.

Global stability analysis of endemic equilibrium point

Theorem 4.4. If $\mathcal{R}_0 > 1$, then the endemic equilibrium point (\mathcal{E}^{**}) of the system (2) is globally asymptotically stable in the region Ω_R .

Proof. Suppose that $\mathcal{R}_0 > 1$ for which (\mathcal{E}^{**}) exits, for checking stability we define the Lyapunov Function $\mathcal{V}_{\mathcal{F}}$. Consider the class Q_s and R as redundant classes.

$$\mathcal{V}_{\mathcal{F}} = (S - S^* - S^* \ln S) + (U - U^* - U^* \ln U) + (M - M^* - M^* \ln M)
+ \mathcal{D}_1(E - E^* - E^* \ln E) + \mathcal{D}_2(I_s - I_s^* - I_s^* \ln I_s) + \mathcal{D}_3(I_a - I_a^* - I_a^* \ln I_a),$$
(23)

where \mathcal{D}_1 , \mathcal{D}_2 and \mathcal{D}_3 are the constants to be determined. We now show that $\frac{d\mathcal{V}_{\mathcal{F}}}{dt} \leq 0$. The time derivative of $\mathcal{V}_{\mathcal{F}}$ is given by

$$\dot{\mathcal{V}_{\mathcal{F}}} = \left(1 - \frac{S^*}{S}\right)\dot{S} + \left(1 - \frac{U^*}{U}\right)\dot{U} + \left(1 - \frac{M^*}{M}\right)\dot{M} + \mathcal{D}_1\left(1 - \frac{E^*}{E}\right)\dot{E} + \mathcal{D}_2\left(1 - \frac{I_s^*}{I_s}\right)\dot{I}_s + \mathcal{D}_3\left(1 - \frac{I_a^*}{I_a}\right)\dot{I}_a.$$

$$(24)$$

At the endemic equilibrium, the steady state solutions of system (7) yield:

$$\alpha = \frac{\pi}{S^*} - \mu, \quad \alpha \rho^* = (\mu + \psi^*) \frac{U^*}{S^*}, \quad \alpha (1 - \rho^*) = (\mu + (1 - \tau)\psi^*) \frac{M^*}{S^*},$$

$$\psi^* = \beta^* (I_a^* + \eta I_s^*), \quad \pi = (\mu + \alpha) S^*, \quad \mathcal{Q}_2 = \psi^* \frac{U^*}{E^*} + (1 - \tau)\psi^* \frac{M^*}{E^*},$$

$$\mathcal{Q}_3 = \frac{\epsilon \kappa E^*}{I_s^*}, \quad \mathcal{Q}_4 = \frac{\epsilon (1 - \kappa) E^*}{I_a^*}.$$
(25)

Substituting the set of Equations from (25) into (24) after some algebraic manipulation it gives,

$$\dot{\mathcal{V}}_{\mathcal{F}} = -\left(\frac{\mu}{S}\right)\left(S - S^{*}\right)^{2} + P_{0}\left(2 - p - \frac{1}{p}\right) + \mu U^{*}\left(2 - \frac{1}{q} - q\right) + P_{1}\left(1 - \frac{1}{q} - qz + z\right) \\
+ P_{2}\left(1 - qy - \frac{1}{q} + y\right) + \mu M^{*}\left(2 - w - \frac{1}{w}\right) + P_{3}\left(1 - wz - \frac{1}{w} + z\right) \\
+ P_{4}\left(1 - wy - \frac{1}{w} + y\right) + \mathcal{D}_{1}P_{1}\left(qz - \frac{qz}{x} - x + 1\right) + \mathcal{D}_{1}P_{2}\left(qy - \frac{qy}{x} - x + 1\right) \\
+ \mathcal{D}_{1}P_{3}\left(wz - \frac{wz}{x} - x + 1\right) + \mathcal{D}_{1}P_{4}\left(wy - \frac{wy}{x} - x + 1\right) + \mathcal{D}_{2}P_{5}\left(x - \frac{x}{y} - y + 1\right) \\
+ \mathcal{D}_{3}P_{6}\left(x - \frac{x}{z} - z + 1\right).$$

The coefficients of x, y, z, qy, qz, wy, and wz are thus set to zero and solved for the values of \mathcal{D}_1 , \mathcal{D}_2 , and \mathcal{D}_3 . We obtain

$$\mathcal{D}_1 = 1, \quad \mathcal{D}_2 = \frac{P_2 + P_4}{P_5}, \quad \mathcal{D}_3 = \frac{P_1 + P_3}{P_6}.$$
 (26)

After using (26) in the above, we obtained

$$\dot{\mathcal{V}}_{\mathcal{F}} = -\left(\frac{\mu}{S}\right) \left(S - S^*\right)^2 + P_0 \left(2 - p - \frac{1}{p}\right) + \mu U^* \left(2 - \frac{1}{q} - q\right) + \mu M^* \left(2 - w - \frac{1}{w}\right) + f_1 - f_2,$$
(27)

$$f_{1} = P_{1} \left(4 - \frac{p}{q} - \frac{qz}{x} - \frac{x}{z} - \frac{1}{p} \right) + P_{2} \left(4 - \frac{p}{q} - \frac{qy}{x} - \frac{x}{y} - \frac{1}{p} \right) + P_{3} \left(4 - \frac{p}{w} - \frac{wz}{x} - \frac{x}{z} - \frac{1}{p} \right) + P_{4} \left(4 - \frac{p}{w} - \frac{wy}{x} - \frac{x}{y} - \frac{1}{p} \right),$$
 (28)

$$f_2 = \left(P_1 + P_2 + P_3 + P_4\right) \left(2 - p - \frac{1}{p}\right). \tag{29}$$

In order to prove that $\dot{\mathcal{V}}_{\mathcal{F}} \leq 0$. Already the first term $-\left(\frac{\mu}{S}\right)\left(S - S^*\right)^2 \leq 0$. Our only task is to prove that the remaining terms are all non-positive. By the arithmetic mean, geometric mean inequality

$$-4 \ge \left(-\frac{p}{w} - \frac{wz}{x} - \frac{x}{z} - \frac{1}{p}\right).$$

Hence, by the GM-AM inequality, the expressions in f_1 are negative. So $f_1 \leq 0$, also $f_1 \leq f_2$. Therefore, $f \leq 0$, and equality holds if and only if p = q = x = z = 1. We prove that all the terms of $\dot{\mathcal{V}}_{\mathcal{F}}$ in (27) are non-positive. So $\mathcal{V}_{\mathcal{F}}$ is positive definite at the endemic equilibrium and $\frac{d\mathcal{V}_{\mathcal{F}}}{dt} \leq 0$ with $\frac{d\mathcal{V}_{\mathcal{F}}}{dt} = 0$ if and only if $S = S^*$, $U = U^*$, $M = M^*$, $E = E^*$, $I_s = I_s^*$, $I_a = I_a^*$, The only invariant set in $\Omega_{R_+^8}$ is the set that contains only the endemic equilibrium point. This shows that each solution intersects R_+^8 limit to the endemic equilibrium. Therefore, the largest invariant set where $\dot{\mathcal{V}}_{\mathcal{F}} = 0$ is the singleton of EE. According to Lasalle's Invariance Principle [23], EE is therefore globally asymptotically stable in an invariant region Ω_R for $\mathcal{R}_0 > 1$.

5. Simulations

Sensitivity analysis

Sensitivity analysis identifies the parameters that most significantly influence \mathcal{R}_0 and disease persistence. The roles of mask efficacy, symptomatic fraction, and quarantine rate are highlighted using partial derivatives, contour plots, and normalized forward sensitivity indices, which quantify the relative change in \mathcal{R}_0 resulting from a relative change in each parameter. These results help to determine the most effective intervention targets.

Definition 5.1. From [24], the normalized sensitivity index of reproductive number \mathcal{R}_0 , which depends differentiably on a parameter h, is defined by an implicit formula for \mathcal{R}_0 ,

 $\gamma_h^{\mathcal{R}_0} = \frac{\partial \mathcal{R}_0}{\partial h} \times \frac{h}{\mathcal{R}_0}.$ (30)

Sensitivity indices of \mathcal{R}_0 to parameters for COVID-19 model, evaluated at baseline parameter values presented in Table 1.

Table 1: Parameter values used in the COVID-19 model with $\mathcal{R}_0 = (0.686, 2.05)$ and corresponding sensitivity indices of \mathcal{R}_0 evaluated at the baseline parameter values.

ues.			
Parameters	Values	Source	Sensitivity Indices
π	$3118 \; (day^{-1})$	calculated	1
μ	$4.3 \times 10^{-5} \ (day^{-1})$	calculated	-0.99
α	(0.006, 0.008)	[14, 25]	0.005
ho	0.4	[14, 26]	0.375
β	$(1.45 \times 10^{-8}, 3 \times 10^{-8})$	assumed	assumed
η	1.44	[27]	0.79
au	0.6	assumed	-0.46
ϵ	0.006	[28]	0.006
κ	0.6	assumed	0.47
ξ	(0.1493, 1.4286)	[29]	-0.53
γ_1	0.583	[14]	0.58
γ_3	0.04	assumed	-0.53

Impact of parameters on the \mathcal{R}_0 .

The influence of critical epidemiological and behavioral parameters on the basic reproduction number, \mathcal{R}_0 , was investigated using contour plots. Among the parameters examined, the transmission rate β , awareness sensitivity κ , mask usage rate τ , and quarantine response ξ were identified as the most influential determinants of disease spread. The analysis demonstrates that \mathcal{R}_0 decreases with increasing mask usage (τ), underscoring the pivotal role of widespread mask adoption in curbing transmission. Conversely, \mathcal{R}_0 rises with a greater proportion of symptomatic individuals and an elevated force of infection, while enhanced mask efficacy contributes to its decline. These results highlight the continued importance of non-pharmaceutical interventions (NPIs) in reducing COVID-19 transmission. From Table 1: η has a significant positive effect as increasing η increases \mathcal{R}_0 , increasing mask efficacy τ reduces \mathcal{R}_0 . β has strongest effect, reducing transmission by masking is most effective. Figure 5(a) indicates that an increase in the proportion of symptomatic individuals leads to an elevation in \mathcal{R}_0 , whereas improved mask efficacy significantly reduces it. In Figure 5(b), a higher force of infection is

associated with an increase in \mathcal{R}_0 ; however, this effect can be mitigated through improvements in mask efficacy. Figure 5(c) further reveals that although an increase in screened cases initially elevates \mathcal{R}_0 , this can be counterbalanced by a rise in quarantined individuals receiving treatment, thereby suppressing \mathcal{R}_0 and enhancing disease control.

Numerical simulations

Numerical results are carried out using parameter values from the various literature; see Table 1. The initial data values are based on the statistics of South Africa's initial total population in 2022, estimated at 59,890,000 [30]. The life expectancy in South Africa is approximated as $\mu = \frac{1}{64.38 \times 365}$ day⁻¹, and the birth rate in 2022 was 0.019. The recruitment rate is as $\pi = 3118$ per day [14]. The initial conditions for the state variables are calculated from different sources as indicated in this section. Initial values S = 28,241,051, U = 11,296,420, and M=16,944,631, based on reasonable assumptions, while the initial values for other state variables were computed accordingly. As of May 30, 2022, laboratoryconfirmed COVID-19 cases in South Africa were reported as $I_s = 481,537$ [31]. The number of asymptomatic individuals was estimated to be approximately 24% of the symptomatic cases, yielding $I_a = 115,569$ [32]. Additionally, hospitalized individuals constituted 41.3% of I_s , resulting in $Q_s = 198,875$ as of May 28, 2022. The exposed population was estimated at E = 1,791,318 [33]. Furthermore, approximately 97% of the population had recovered, leading to R = 820,599 [34]. According to [35], the elderly population in South Africa accounts for approximately 3% of the total. Wearing masks effectively reduces both contact rates and infection probabilities, particularly among vulnerable populations such as the elderly and immunosuppressed individuals. Our analysis indicates that if at least 72% of the population adopts mask usage, the basic reproduction number satisfies $\mathcal{R}_0 < 1$, ultimately leading to disease eradication. (Figure 6a), (Figure 7a), and (Figure 8a) show that increased awareness, increased number of quarantined individuals, and higher mask efficacy contribute to controlling the spread of the disease. (Figure 6b), (Figure 7b), and (Figure 8b) illustrate that if asymptomatic individuals adopt precautionary measures such as wearing masks, it can significantly enhance their recovery. The impact of mask efficacy on asymptomatic individuals reveals an inverse correlation. An increase in mask efficacy reduces asymptomatic infections, demonstrating the effectiveness of masks in controlling disease spread. Moreover, mask usage among asymptomatic individuals helps lower the contact rate, thereby limiting transmission. A decrease in the infection rate fosters a controlled environment for individuals affected by COVID-19. Conversely, if the infection rate increases, the model dynamics show that the threshold value also rises, signifying a substantial increase in disease spread as \mathcal{R}_0 surpasses one. On the other hand, a reduction in the infection rate results in $\mathcal{R}_0 < 1$, indicating effective disease control. Even when relying solely on non-pharmaceutical interventions such as mask usage, reducing infection rates leads to a correspond-

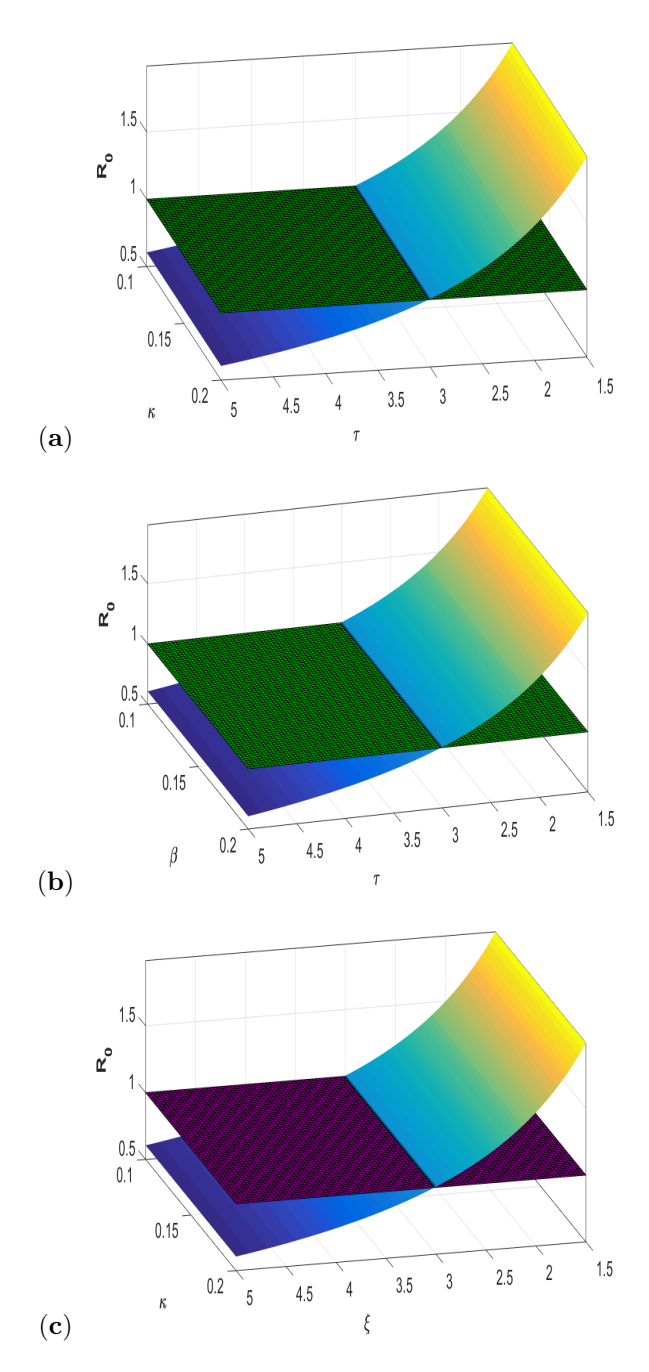


Figure 5: Contour plots of \mathcal{R}_0 . (a) Screened individuals vs the efficacy of masks. (b) Infection rate vs efficacy of masks. (c) Screened vs quarantined individuals.

ing decline in the number of infected individuals, aiding in disease mitigation. Additionally, an increase in κ significantly influences the dynamics of the infected population. As κ rises, COVID-19 prevalence also increases. However, regardless of the proportion of individuals transitioning into the infected compartment, the disease will persist in the human population but remain controllable, ultimately stabilizing as an endemic condition. The following figures illustrate the model dynamics in response to these factors.

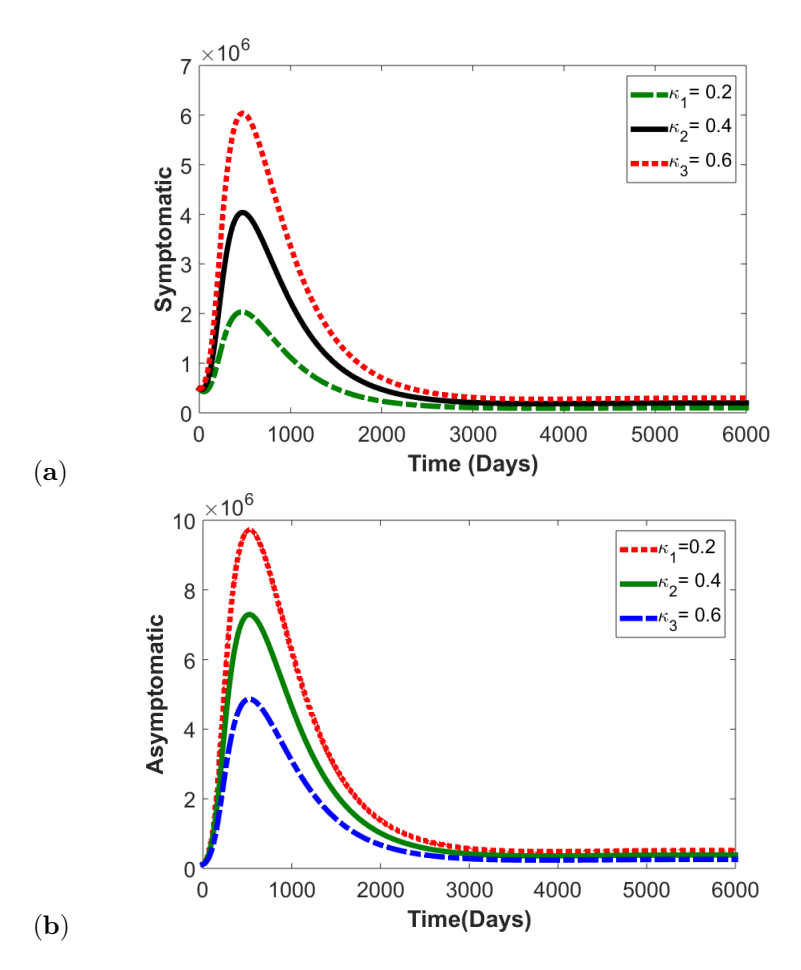


Figure 6: Analytical impact of rate of screened or tested positive on (a) Symptomatic I_s , (b) Asymptomatic I_a , individuals of COVID-19 in South Africa.

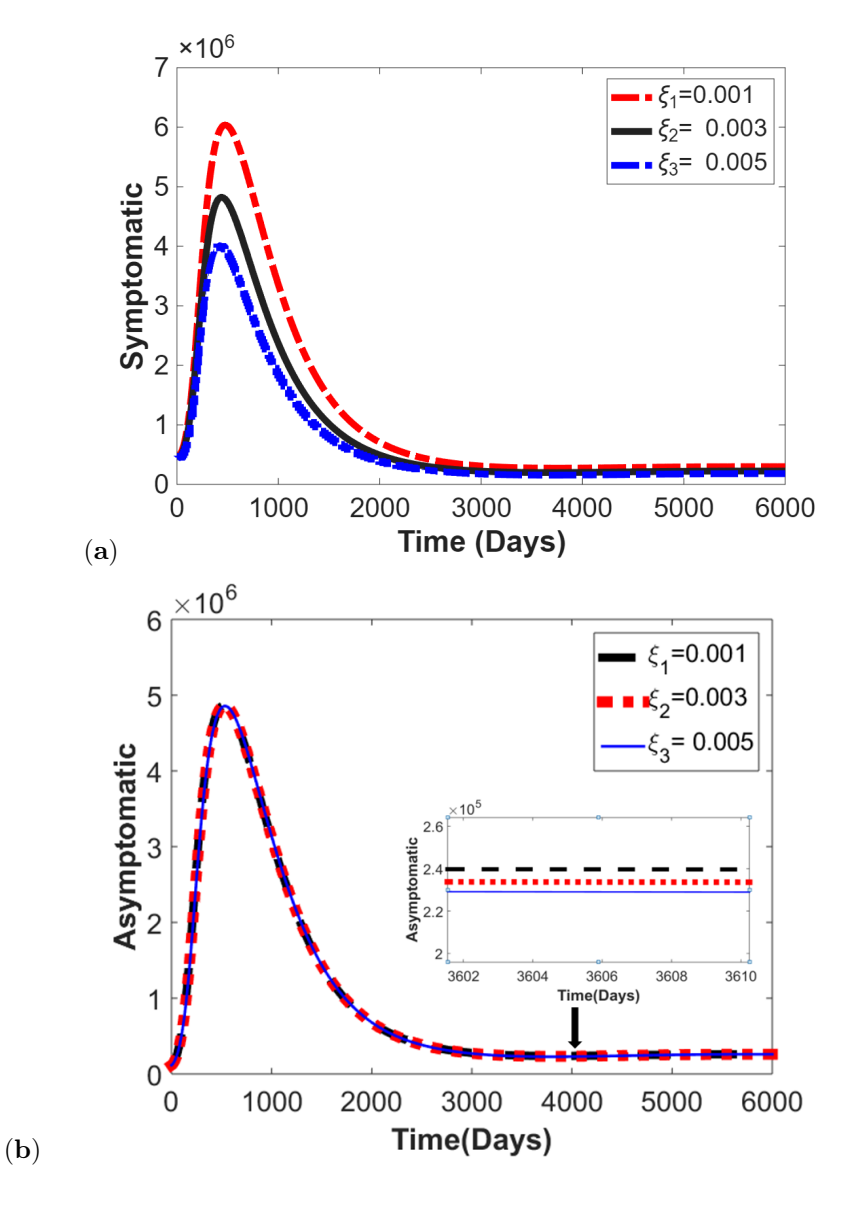


Figure 7: Analytical behavior of rate of quarantined individuals, (a) Symptomatic I_s , (b) Asymptomatic I_a , individuals of COVID-19 in South Africa.

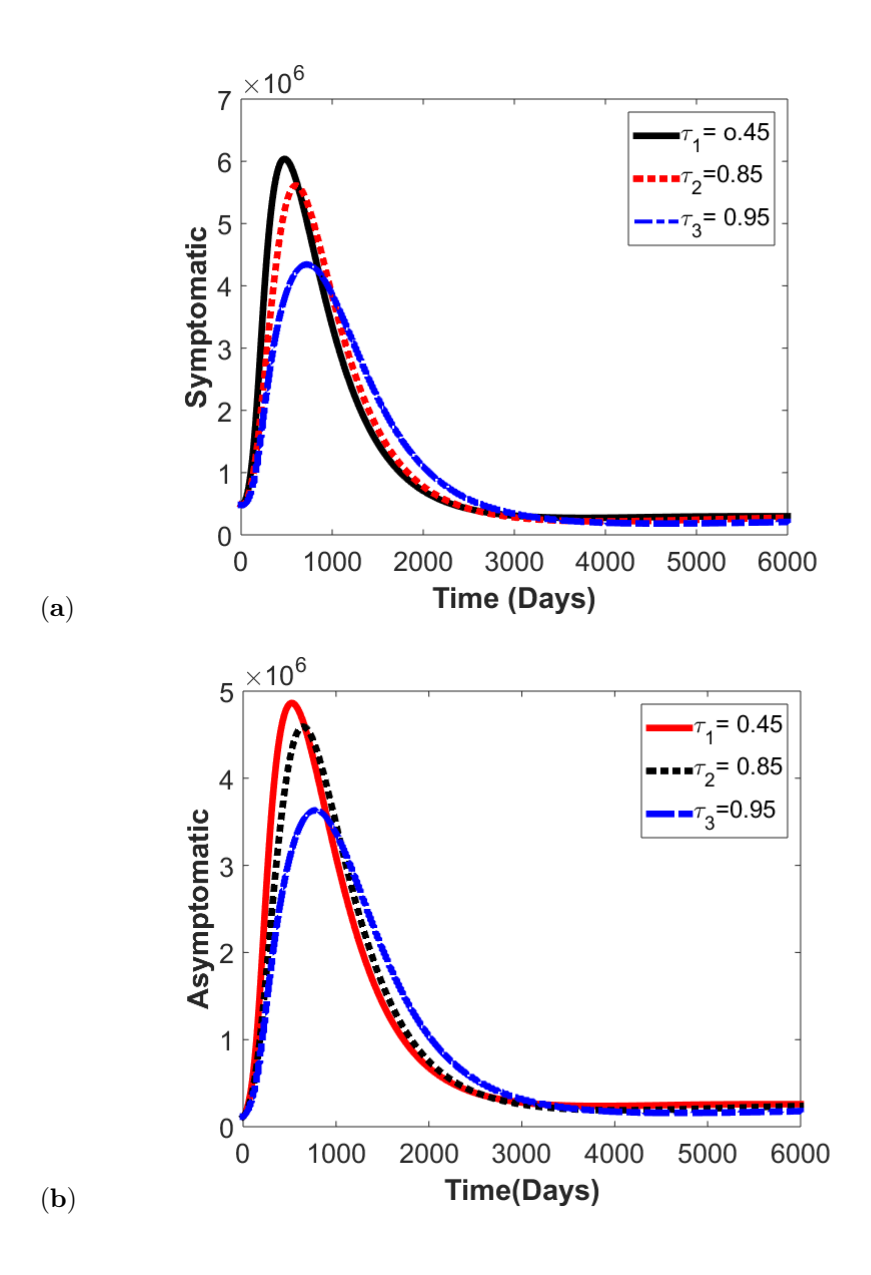


Figure 8: Analytical impact of efficacy of mask on (a) Symptomatic I_s , (b) Asymptomatic I_a , individuals of COVID-19 in South Africa.

Results and discussion

This study presents a refined deterministic compartmental model, the $SUMEI_sI_aQ_sR$ model, to give insights on the transmission dynamics of COVID-19 in South Africa, with a focused investigation into the synergistic effects of mask-wearing and quarantine. The model provides both theoretical insights and practical public health implications, offering a deeper understanding of how non-pharmaceutical interventions interact to influence epidemic outcomes.

The work introduces a refined epidemic model that integrates two key interventions: population-level mask usage, distinguishing between masked and unmasked susceptible, and quarantine of symptomatic individuals, enabling a detailed analysis of their combined impact on transmission dynamics, beyond earlier models that treated these strategies separately. The model rigorously defines the basic reproduction number, R_0 , as the epidemic threshold and shows that the disease-free equilibrium is locally asymptotically stable when $R_0 < 1$, while sustained transmission occurs when $R_0 > 1$. Furthermore, a transcritical bifurcation at $R_0 = 1$ and the potential for a backward bifurcation, where a stable endemic equilibrium coexists with the disease-free state for $R_c < R_0 < 1$, imply that merely reducing R_0 below unity is insufficient for eradication, necessitating early and aggressive interventions to suppress infections below a critical threshold.

The analytical expression for R_0 explicitly incorporates mask efficacy (τ) and the proportion of the population using masks $(1-\rho)$. Numerical simulations indicate that a compliance rate of at least 72% is necessary to achieve $R_0 < 1$ and prevent large-scale outbreaks, providing a concrete target for public health policy. Contour plots illustrate how high mask efficacy mitigates the heightened risk from stronger transmission or a larger symptomatic population. For $R_0 > 1$, a Lyapunov function establishes that the endemic equilibrium is globally asymptotically stable, confirming that in the absence of sufficient interventions, the disease will persist. Sensitivity analysis further reveals that the transmission rate (β) is the most influential parameter, followed by mask efficacy (τ) and the proportion of unmasked individuals (ρ) . These findings underscore the critical role of widespread mask use and social distancing, supported by enhanced quarantine and recovery measures, as a hierarchy of interventions for effective control.

While the model provides valuable insights, it is subject to several limitations that suggest directions for future work. The assumption of a homogeneous, well-mixed population ignores heterogeneities in contact structure, age distribution, and spatial clustering, all of which strongly influence transmission. Moreover, waning immunity and the potential for reinfection are omitted; incorporating these processes would be essential for long-term projections and assessing the role of booster vaccinations. Finally, the parameter estimates were calibrated to a specific phase of the pandemic. Fitting the model to time-series data across multiple epidemic waves, including those driven by new variants, would strengthen its predictive capacity. Addressing these limitations would enhance the model's utility as a decision-support tool for public health planning and policy formulation with

respect to COVID-19.

Conflicts of Interest. The authors declare that they have no conflicts of interest regarding the publication of this article.

References

- [1] World Health Organization, Coronavirus disease COVID-19 pandemic, WHO, Available at: https://www.who.int/emergencies/diseases/novel-coronavirus-2019, Accessed 15 July 2022.
- [2] M. Ali, S. T. H. Shah, M. Imran and A. Khan, The role of asymptomatic class, quarantine and isolation in the transmission of COVID-19, *J. Biol. Dyn.* **14** (2020) 389 408, https://doi.org/10.1080/17513758.2020.1773000.
- [3] S. P. Gatyeni, F. Chirove and F. Nyabadza, Modelling the potential impact of stigma on the transmission dynamics of COVID-19 in South Africa, *Mathematics* **10** (2022) #3253, https://doi.org/10.3390/math10183253.
- [4] S. Khajanchi and K. Sarkar, Forecasting the daily and cumulative number of cases for the COVID-19 pandemic in India, *Chaos* 30 (2020) #071101, https://doi.org/10.1063/5.0016240.
- [5] S. Khajanchi, K. Sarkar, J. Mondal, K. S. Nisar and S. F. Abdelwahab, Mathematical modeling of the COVID-19 pandemic with intervention strategies, Results Phys. 25 (2021) #3104285, https://doi.org/10.1016/j.rinp.2021.104285.
- [6] P. Samui, J. Mondal and S. Khajanchi, A mathematical model for COVID-19 transmission dynamics with a case study of India, *Chaos Solitons Fractals* **140** (2020) #110173, https://doi.org/10.1016/j.chaos.2020.110173.
- [7] R. Kumar Rai, P. Kumar Tiwari and S. Khajanchi, Modeling the influence of vaccination coverage on the dynamics of COVID-19 pandemic with the effect of environmental contamination, *Math. Methods Appl. Sci.* **46** (2023) 12425 12453, https://doi.org/10.1002/mma.9185.
- [8] K. Sarkar, J. Mondal and S. Khajanchi, How do the contaminated environment influence the transmission dynamics of COVID-19 pandemic?, Eur. Phys. J. Spec. Top. 231 (2022) 3697 3716, https://doi.org/10.1140/epjs/s11734-022-00648-w.
- [9] R. K. Rai, S. Khajanchi, P. K. Tiwari, E. Venturino and A. K. Misra, Impact of social media advertisements on the transmission dynamics of COVID-19 pandemic in India, J. Appl. Math. Comput. 68 (2022) 19 – 44, https://doi.org/10.1007/s12190-021-01507-y.

- [10] S. Khajanchi, K. Sarkar and J. Mondal, Dynamics of the COVID-19 pandemic in India, arXiv preprint (2020) https://arxiv.org/abs/2005.06286.
- [11] M. A. Khan and Fatmawati, Dengue infection modeling and its optimal control analysis in East Java, Indonesia, *Heliyon* **7** (2021) #e06023, https://doi.org/10.1016/j.heliyon.2021.e06023.
- [12] S. He, Y. Peng and K. Sun, SEIR modeling of the COVID-19 and its dynamics, Nonlinear Dyn. **101** (2020) 1667 1680, https://doi.org/10.1007/s11071-020-05743-y.
- [13] M. A. Khan, A. Atangana, E. Alzahrani and Fatmawati, The dynamics of COVID-19 with quarantined and isolation, *Adv. Difference Equ.* **2020** (2020) #425, https://doi.org/10.1186/s13662-020-02882-9.
- [14] A. J. Mumbu and A. K. Hugo, Mathematical modelling on COVID-19 transmission impacts with preventive measures: a case study of Tanzania, J. Biol. Dyn. 14 (2020) 748 766, https://doi.org/10.1080/17513758.2020.1823494.
- [15] Y. A. Adebisi, A. Ekpenyong, B. Ntacyabukura, M. Lowe, N. D. Jimoh, T. O. Abdulkareem and D. E. Lucero-Prisno, COVID-19 highlights the need for inclusive responses to public health emergencies in Africa, Am. J. Trop. Med. Hyg. 104 (2020) 449 452, https://doi.org/10.4269/ajtmh.20-1485.
- [16] BBC News, COVID-19 pandemic data/South Africa medical cases, *BBC*, Available at: https://www.bbc.com/news/world-asia-china, Accessed 25 July 2022.
- [17] J. Kew, Covid-19 deaths pass 700,000; WHO to send 43 specialists to SA, *BizNews*, Available at: https://www.biznews.com/inside-covid-19/2020/08/05/covid-19-deaths, Accessed 26 July 2022.
- [18] S. P. Gatyeni, C. W. Chukwu, F. Chirove, Fatmawati and F. Nyabadza, Application of optimal control to the dynamics of COVID-19 disease in South Africa, *Sci. Afr.* **16** (2022) #e01268, https://doi.org/10.1016/j.sciaf.2022.e01268.
- [19] M. L. Juga, Modelling the Ebola virus disease dynamics in the presence of interference of interventions, UJ. Master's thesis, University of Johannesburg, South Africa, 2020.
- [20] M. A. Khan, N. Ozdemir, I. Ahmad, N. M. Isa and E. Alzahrani, Modeling and analysis of HIV/AIDS spread in Pakistan: Role of optimal control and behavioral changes, J. Comput. Appl. Math. 473 (2026) #116913, https://doi.org/10.1016/j.cam.2025.116913.
- [21] J. D. Murray, Mathematical Biology: I. An Introduction, Springer, New York, NY, 2007.

- [22] C. Castillo-Chavez and B. Song, Dynamical models of tuberculosis and their applications, $Math.~Biosci.~Eng.~\mathbf{1}$ (2004) 361-404, https://doi.org/10.3934/mbe.2004.1.361.
- [23] J. L. Salle and S. Lefschetz, Stability by Liapunov's Direct Method: With Applications, Academic Press, New York-London, 1961.
- [24] N. Chitnis, J. M. Hyman and J. M. Cushing, Determining important parameters in the spread of malaria through the sensitivity analysis of a mathematical model, *Bull. Math. Biol.* **70** (2008) 1272 1296, https://doi.org/10.1007/s11538-008-9299-0.
- [25] M. A. Khan and A. Atangana, Modeling the dynamics of novel coronavirus (2019-nCov) with fractional derivative, Alex. Eng. J. 59 (2020) 2379 – 2389, https://doi.org/10.1016/j.aej.2020.02.033.
- [26] T.-M. Chen, J. Rui, Q.-P. Wang, Z.-Y. Zhao, J.-A. Cui and L. Yin, A mathematical model for simulating the phase-based transmissibility of a novel coronavirus, *Infect Dis Poverty* 9 (2020) #24, https://doi.org/10.1186/s40249-020-00640-3.
- [27] D. McEvoy, C. McAloon, A. Collins, K. Hunt, F. Butler, A. Byrne, M. Casey-Bryars, A. Barber, J. Griffin, E. A. Lane, P. Wall and S. J. More, Relative infectiousness of asymptomatic SARS-CoV-2 infected persons compared with symptomatic individuals: a rapid scoping review, BMJ Open 11 (2021) #e042354, https://doi.org/10.1136/bmjopen-2020-042354.
- [28] S. A. Lauer, K. H. Grantz, Q. Bi, F. K. Jones, Q. Zheng, H. R. Meredith, A. S. Azman, N. G. Reich and J. Lessler, The incubation period of coronavirus disease 2019 (COVID-19) from publicly reported confirmed cases: estimation and application, *Ann. Intern. Med.* 172 (2020) 577 582, https://doi.org/10.7326/M20-0504.
- [29] B. Ivorra, M. R. Ferrández, M. Vela-Pérez and A. M. Ramos, Mathematical modeling of the spread of the coronavirus disease 2019 (COVID-19) taking into account the undetected infections: The case of China, Commun. Nonlinear Sci. Numer. Simul. 88 (2020) #105303, https://doi.org/10.1016/j.cnsns.2020.105303.
- [30] Statistics South Africa, $Stats\ SA$, Available at https://www.statssa.gov.za/? p=16711 #::text.
- [31] Worldometer, COVID-19 Coronavirus Pandemic, South Africa, Available at: https://www.worldometers.info/coronavirus/, Accessed 30 July 2024.
- [32] X. Chen, Z. Huang, J. Wang, S. Zhao, M. C.-S. Wong, K. C. Chong, D. He and J. Li, Ratio of asymptomatic COVID-19 cases among ascertained SARS-CoV-2 infections in different regions and population groups in 2020: A systematic

- review and meta-analysis including 130, 123 infections from 241 studies, BMJ Open. 11 (2021) #e049752, https://doi.org/10.1136/bmjopen-2021-049752.
- [33] C. Maslo, R. Friedland, M. Toubkin, A. Laubscher, T. Akaloo and B. Kama, Characteristics and outcomes of hospitalized patients in South Africa during the COVID-19 Omicron wave compared with previous waves, *JAMA*. 327 (2022) 583 – 584, https://doi.org/10.1001/jama.2021.24868.
- [34] F. Wilta, A. L. C. Chong, G. Selvachandran, K. Kotecha and W. Ding, Generalized susceptible—exposed—infectious—recovered model and its contributing factors for analysing the death and recovery rates of the COVID-19 pandemic, *Appl. Soft Comput.* **123** (2022) #108973, https://doi.org/10.1016/j.asoc.2022.108973.
- [35] Department of Statistics, South Africa, Protecting South Africa's elderly, SSA, Available at: https://www.statssa.gov.za/?p=13445, Accessed 15 July 2023.

Farah Naz
Department of Mathematics and Applied Mathematics,
University of Johannesburg,
Auckland Park 2006,
South Africa
e-mail: farahn@uj.ac.za

Farai Nyabadza
Department of Mathematics and Applied Mathematics,
University of Johannesburg,
Auckland Park 2006,
South Africa

and

Institute of Applied Research and Technology, Emirates Aviation University, Dubai International Academic City, United Arab Emirates e-mail: fnyabadza@uj.ac.za